THE JOURNAL OF COMPARATIVE NEUROLOGY 494:381–397 (2006)

Morphology, Characterization, and Distribution of Retinal Photoreceptors in the Australian Lungfish *Neoceratodus forsteri* (Krefft, 1870)

HELENA J. BAILES,[1]* STEPHEN R. ROBINSON,[2] ANN E.O. TREZISE,[1] AND SHAUN P. COLLIN[1]

[1]School of Biomedical Sciences, The University of Queensland, St. Lucia, Queensland 4072, Australia

[2]Department of Psychology, Monash University, Clayton, Victoria 3800, Australia

ABSTRACT

The Australian lungfish *Neoceratodus forsteri* (Dipnoi) is an ancient fish that has a unique phylogenetic relationship among the basal Sarcopterygii. Here we examine the ultrastructure, histochemistry, and distribution of the retinal photoreceptors using a combination of light and electron microscopy in order to determine the characteristics of the photoreceptor layer in this living fossil. Similar proportions of rods (53%) and cones (47%) reveal that *N. forsteri* optimizes both scotopic and photopic sensitivity according to its visual demands. Scotopic sensitivity is optimized by a tapetum lucidum and extremely large rods (18.62 ± 2.68 μm ellipsoid diameter). Photopic sensitivity is optimized with a theoretical spatial resolving power of 3.28 ± 0.66 cycles degree^{-1}, which is based on the spacing of at least three different cone types: a red cone containing a red oil droplet, a yellow cone containing a yellow ellipsoidal pigment, and a colorless cone containing multiple clear oil droplets. Topographic analysis reveals a heterogeneous distribution of all photoreceptor types, with peak cone densities predominantly found in temporal retina (6,020 rods mm^{-2}, 4,670 red cones mm^{-2}, 900 yellow cones mm^{-2}, and 320 colorless cones mm^{-2}), but ontogenetic changes in distribution are revealed. Spatial resolving power and the diameter of all photoreceptor types (except yellow cones) increases linearly with growth. The presence of at least three morphological types of cones provides the potential for color vision, which could play a role in the clearer waters of its freshwater environment. J. Comp. Neurol. 494: 381–397, 2006.

Indexing terms: color vision; Dipnoi; oil droplets; spatial resolving power; sensitivity; ontogeny

The Australian lungfish *Neoceratodus forsteri* is the sole surviving species representing the family Ceratodontidae (order Dipnoi). The dipnoan order arose during the Devonian period 410 million years ago (m.y.a.) (Moy-Thomas and Miles, 1971), and all three living genera (*N. forsteri*, *Lepidosiren paradoxa* from South America and *Protopterus* spp. from Africa) have a fossil record dating back to the Cretaceous era (Sige, 1968; Broin et al., 1974; Kemp and Molnar, 1981; Marshall, 1986). *N. forsteri* is believed to be the most primitive representative, having changed little in body morphology over the last 100 million years (Kemp and Molnar, 1981). Lungfish are heavy-bodied, large freshwater fish with lobed fins and the ability to breathe air with a modified lung. Although the three genera are now spread over a large (yet fragmented) geographical area, they inhabit similar environments i.e., slow moving freshwater rivers in South America, Africa,

Grant sponsor: the Australian Research Council Discovery Grant; Grant number: DP0209452 (to S.P.C., H.J.B., S.R.R., A.E.O.T.); Grant sponsor: University of Queensland International Postgraduate Research scholarship (to H.J.B.); Grant sponsor: University of Queensland Graduate School Research Travel Award (to H.J.B.).

*Correspondence to: Helena J. Bailes, Anatomy and Developmental Biology, School of Biomedical Sciences, University of Queensland, St. Lucia, Brisbane, QLD 4072, Australia.
E-mail: h.bailes@uq.edu.au

Received 16 March 2005; Revised 6 July 2005; Accepted 16 August 2005

DOI 10.1002/cne.20809

Published online in Wiley InterScience (www.interscience.wiley.com).

and Australia. Within Australia, *N. forsteri* is resident in only four rivers in South East Queensland and is protected by Australian law and the Convention on International Trade of Endangered Species (CITES).

The exact relationship between the Dipnoi, Crossopterygii (represented by the coelacanth, *Latimeria* sp.) and the tetrapods remains controversial, with recent molecular evidence favoring a lungfish and tetrapod clade (Yokobori et al., 1984; Tohyama et al., 2000; Venkatesh et al., 2001; Brinkmann et al., 2004). Results can vary greatly depending on the nature of the gene under investigation or the phylogenetic method employed, with a coelacanth/lungfish or lungfish/tetrapod clade often equally supported on molecular grounds (Zardoya et al., 1998; Joss et al., 2001; Takezaki et al., 2004). The continued uncertainty regarding the phylogeny of the Dipnoi and their relationship to the tetrapods makes further research into the anatomy and physiology of members of this order essential in revealing relationships among basal sarcopterygiians.

Dean (1906) declared that vision is of little importance to *N. forsteri* due to their sluggish behavior in captivity. Based on a relatively small eye size (reaching a maximum of 1.5 cm in diameter in an adult 127 cm total length; unpublished data), later studies on the biology of this living fossil similarly considered that the visual system played only a minor role in survival (Kemp, 1986; Simpson et al., 2002). Although it has been shown that *N. forsteri* uses electroreception to locate prey hidden beneath the substrate (Watt et al., 1999), parts of the freshwater rivers it inhabits are relatively clear, suggesting that vision may also play an important role, especially in foraging. Unfortunately, there are no behavioral studies of vision in lungfish, and our knowledge of the role of vision is based on a few early studies of ocular anatomy.

The retinae of the South American and African lungfish have been described at the level of the light microscope; they possess rods and single cones (*L. paradoxa*) or single and double cones (*Protopterus* sp.), all containing a paraboloid and a clear oil droplet (Kerr, 1902; Rochon-Duvigneaud, 1941; Walls, 1942; Munk, 1964, 1969; Pfeiffer, 1968; Ali and Anctil, 1973). Schiefferdecker (1886) first examined the retina of *N. forsteri* and described single cones containing clear oil droplets and rods without oil droplets. In addition to single cones and rods, Munk (1969) later identified the presence of unequal double cones. Pow (1994) described the ultrastructure of the retina of *N. forsteri* in the context of the localization of amino acid neurotransmitters but only characterized a rod and one type of single cone. Robinson (1994), however, described at least three cone types in *N. forsteri*. The cones were characterized by a red oil droplet, a colorless droplet, or a granular yellow pigment at the base of the outer segment. In addition, cone oil droplets at the edges of some retinae were reported to be orange rather than red. This was the first description of colored oil droplets in the retina of a fish, in which they had previously only been associated with diurnal, highly visual reptiles and birds (Robinson, 1994).

In this study, we wanted to verify the complement of photoreceptor types present in the retina of *N. forsteri* and characterize them based on their size, ultrastructure, histochemistry, and topographic distribution in both juveniles and adults. We reveal at least four distinct photoreceptor types (including a very large rod) distributed heterogeneously across the retina with photoreceptor size and spatial resolving power increasing with growth. These findings have implications for the evolution of color vision and the phylogenetic relationships among the basal sarcopterygians.

MATERIALS AND METHODS

Source and maintenance of animals

Five adults/subadults of *Neoceratodus forsteri* (Ceratodontidae, Dipnoi) were caught on either hook and line or seine net from the Mary and Brisbane Rivers between December 1990 and July 2004 (Queensland Fisheries Management Authority Permit No. PRM01599G). A subadult approx. 70 cm in total length (TL) and a juvenile 6.8 cm in TL were kindly donated by Dr. A. Kemp of the University of Queensland. Juvenile animals between 19 cm and 40 cm in length were generously donated by Prof. J. Joss from Macquarie University, Australia. All animals were maintained in freshwater aquaria at the University of Queensland under a 12:12-hour light/dark cycle and fed a diet of commercial fish food. Adults were euthanized with an overdose (>20 ml/liter) of benzocaine (Sigma-Aldrich, St. Louis, MO) dissolved in acetone (50 g/liter), and spinal cord section was performed in accordance with the animal ethics guidelines of the University of Queensland (AEC no. ANAT/436/04/ARC). Prior to enucleation a lesion was made in the dorsal limbus of the eye for orientation.

Light and electron microscopy

Two retinae (animals 6.8 and 31.5 cm in TL) were processed for both light and electron microscopy. Following enucleation, the cornea and lens were removed, and the tissue was fixed in Karnovsky's solution (2% paraformaldehyde, 2.5% glutaraldehyde in 0.1 M sodium cacodylate buffer pH 7.4) for between 1 and 7 days. Ocular tissue was stored at 4°C in 0.1 M sodium cacodylate buffer prior to further dissection and resin embedding. It was found that removal of the retina from the eyecup prior to resin infiltration resulted in substantial mechanical damage to photoreceptor outer segments, so the retina was removed from the sclera and cut into sections (2 × 5 mm) just prior to embedding in EPON and polymerization. Even employing these methods, the outer segments of adult retinae were often destroyed due to their large size and fragility, so all ultrastructural examination was carried out on juveniles. Semithin and ultrathin sections were cut by using a Leica Ultracut UCT ultramicrotome. Semithin sections were stained with 4% Toluidine blue and examined on a Leica Dialux 20 light microscope. Ultrathin sections were stained with uranyl acetate and lead citrate before examination on a JEOL JEM 1010 transmission electron microscope at 80 KV.

One retina (individual 100 cm in TL) was fixed as above but then dehydrated in a series of ethanols and critical point dried for scanning electron microscopy (SEM). The tissue was then cracked with fine forceps, placed on a specimen stub, and sputter-coated with gold. Samples were examined by using a JEOL JSM 6300F scanning electron microscope at 5 KV. Photomicrographs (TEM and SEM) were taken by using a Megaview III Soft Imaging System digital camera and AnalySIS iTEM software (Soft Imaging System, Münster, Germany). Images were

cropped, and contrast and brightness were altered by using Adobe Photoshop 7.0 for Windows (Adobe Systems, San Jose, CA).

Retinal histochemistry

One retina (individual 52 cm in TL) was originally fixed in 2% gluteraldehyde and 4% paraformaldehyde in 0.1 M phosphate buffer for 24 hours and then stored for 12 years in 0.5% glutaraldehyde in 0.1 M sodium cacodylate buffer. Under these conditions, the oil droplet colors oxidized and appeared colorless. Small strips (3 × 10 mm) of retina were embedded in Tissue-Tek OCT compound (Sakura Finetechnical, Tokyo, Japan) and frozen in liquid nitrogen. Transverse sections were cut by using a Leica CM3050 cryostat and then stained for lipids with Oil Red O, which positively stains triglycerides deep red (Lillie and Ashburn, 1943). Slides containing stained and unstained sections were mounted with Mount-Quick "Aqueous" (United Biosciences, Queensland, Australia) and examined by using an Olympus BX60 light microscope. All photographs of light microscopy were taken with an Olympus DP70 digital camera and DP70-BSW software (Olympus, Tokyo, Japan). Images were cropped, and contrast and brightness were altered by using Adobe Photoshop 7.0 for Windows.

Assessment of photoreceptor dimensions

The ellipsoidal diameter (measured at the widest point), outer segment length, and outer segment base diameter were all measured by using Image J (Rasband, 1997–2005) from a minimum of six randomly selected photoreceptors of each type from individuals with TLs of 6.8, 31.5, 39.5, and 104 cm in light and electron micrographs. Retinal thickness was also measured at five random locations in transverse sections. Minimal shrinkage was observed in retinal tissue that had been lightly fixed or was freshly prepared for wholemounts (see below). However, by comparing photoreceptor dimensions and retinal thickness from fresh tissue and tissue fixed, embedded, and sectioned for transmission electron microscopy, shrinkage was estimated to be 5%. This degree of shrinkage was applied to all photoreceptor measurements taken from different aged individuals other than in fresh wholemounts. All measurements are quoted as mean ± SD followed by sample size (n). The significance of any changes in photoreceptor dimensions between different body sizes was assessed by using an unpaired t-test (between two groups of equal variance) or one-way ANOVA with a post hoc Tukey-Kramer test (among three or more groups). Ontogenetic changes in receptor dimensions were also assessed for the degree of fit to simple linear functions of fish total length. All statistics were calculated by using GraphPad Prism version 4.01 for Windows (GraphPad Software, San Diego, CA).

Assessment of photoreceptor distribution

All ocular tissue used for topographical analysis of photoreceptor distribution was fixed in 4% paraformaldehyde in 0.1 M phosphate buffer (pH 7.4) for 4 hours before the retina was carefully dissected out. Six retinae (from three adults approx. 1 m in TL, one subadult approx. 70 cm in TL, and a juvenile 19 cm in TL) were wholemounted (photoreceptor side up) following numerous radial cuts from the periphery, to ensure the retina was flattened, and mounted in 50% glycerol in 0.1 M phosphate buffer (Stone, 1981). Cell counts were made by using brightfield microscopy with a reduced aperture to enhance contrast at 500× or 630× magnification depending on retinal size. Cell types were identified according to their color and/or size (see Results). The outline of each retina was then traced onto grid paper with any major landmarks noted, and the scale was determined by using a calibrated 0.01-mm micrometer slide. Cell counts were made at regular intervals across the retina by using an eyepiece graticule. A minimum of 0.2% (individual 19 cm in TL) of the retina was sampled, but this was substantially increased (up to 12% in a 98.5 cm TL individual) when the underlying retinal pigment epithelium could effectively be removed.

Cell counts were converted to density counts in cells mm^{-2}, and isodensity contour lines constructed. The first contour line depicts regions above and below the mean cell density for each photoreceptor type, calculated from raw cell counts. A second contour line was included for areas with cell densities more than 1 SD above the mean cell density for that photoreceptor type in that retina (similar to the method used by Beaudet et al., 1997).

Retinal area was calculated from scanned images of the retinal outline by using Image J (Rasband, 1997–2005). Total photoreceptor numbers were calculated by 1) multiplying the mean cell density by the retinal area, and 2) multiplying the median cell density of each retinal contour by the individual retinal area covered by that contour. The results with the two methods were comparable due to the small density gradient across each retina. The ratio of each photoreceptor type as a percentage of the total number of photoreceptors was calculated from retinal wholemounts. Potential spatial resolving power was determined from peak cone densities and estimated by using the formula derived by Tamura (1957): α (radians) = $2c/f$ where α is the minimum separable angle (MSA), c is the distance between the centers of three adjacent cones (because an unstimulated cone between two neighboring cones is required to define a grating), and f is the focal length or posterior nodal distance (PND) of the lens. MSA was converted to degrees (measured in minutes of arc) and then converted to cycles $degree^{-1}$. Matthiessen's ratio was used to calculate the PND. Matthiessen (1880) states that teleost fish possess a spherical lens with a constant relationship between the distance from the lens center to the retina and the lens radius (i.e., PND = 2.55r, where r is the lens radius).

RESULTS

Morphology of the retina and choroid

All the major layers of the vertebrate retina can be differentiated in *Neoceratodus forsteri*, although most cell types are large and the nuclear layers are interposed between relatively thin plexiform layers (Fig. 1A). The entire retina is thin (137.06 ± 2.35 μm in a 6.8-cm TL individual, n = 5, increasing to 192.37 ± 11.27 μm in a 98-cm TL individual, n = 5), and each nuclear layer possesses a maximum of four sublaminae at any retinal locus. There is no retinal or vitreal vasculature.

The choroid is comprised of large choroidal blood vessels and a *rete mirabile* situated within loose connective tissue and interspersed with cells containing reflecting material. Transmission electron microscopy of these tapetal areas

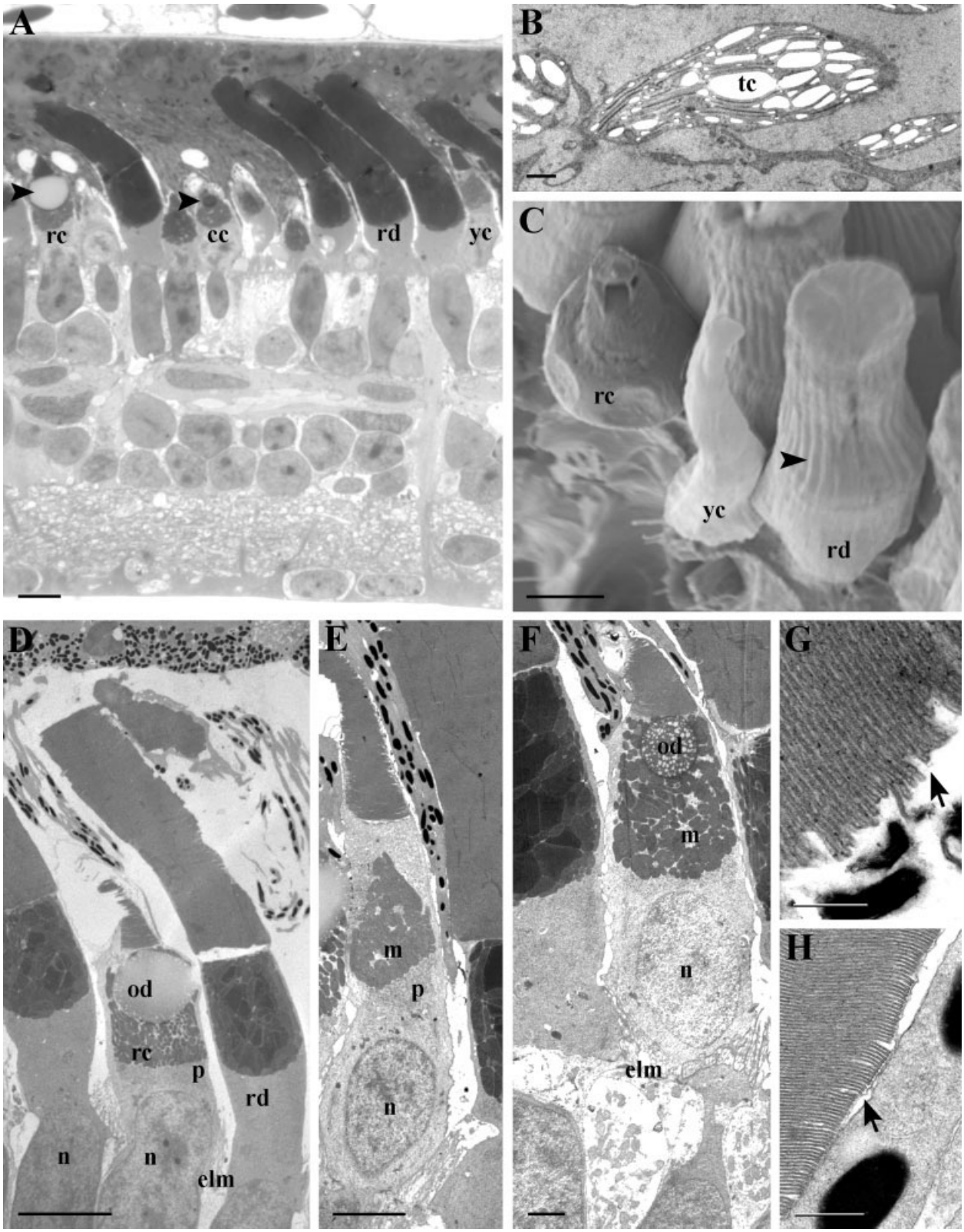

Fig. 1. Light and electron micrographs of photoreceptor characteristics in *Neoceratodus forsteri*. **A:** Light micrograph of a cross section of retina stained with Toluidine blue showing all four morphological types. Rods (rd) are most numerous; red cones (rc) can be identified by their large oil droplet (arrowhead). Yellow cones (yc) have a lightly staining region above the mitochondria; clear cones (cc) have smaller oil droplets (arrowhead) than red cones. **B:** Transmission electron micrograph of the tapetal area with tapetal cells (tc) showing small holes where presumably guanine has dissolved away during processing. Most of the holes are arranged perpendicular to the incoming light path. **C:** Scanning electron micrograph showing three morphological photoreceptor types; a rod and a red and yellow cone. Shading has been artificially altered to enhance the discrimination of photoreceptor types. Calycal processes can be seen spanning the length of the outer segment (arrowhead). **D:** Transmission electron micrograph showing a rod and a red cone and the relative position of their nuclei (n). **E:** Electron micrograph of a yellow cone. **F:** Electron micrograph of a clear cone, with only one oil droplet (od) visible. The nucleus (n) is situated more sclerad than the red cone nucleus. **G:** Electron micrograph of the outer segment disks of a red cone. Note the continuation of the space between disks with the extracellular space (arrow). **H:** Electron micrograph of the outer segment disks of a rod. The disks are surrounded by a plasma membrane (arrow), unlike in the red cone. elm, external limiting membrane; rpe, retinal pigment epithelium. Scale bars = 20 μm in A; 1 μm in B; 5 μm in C,E; 10 μm in D; 2 μm in F; 200 nm in G; 500 nm in H.

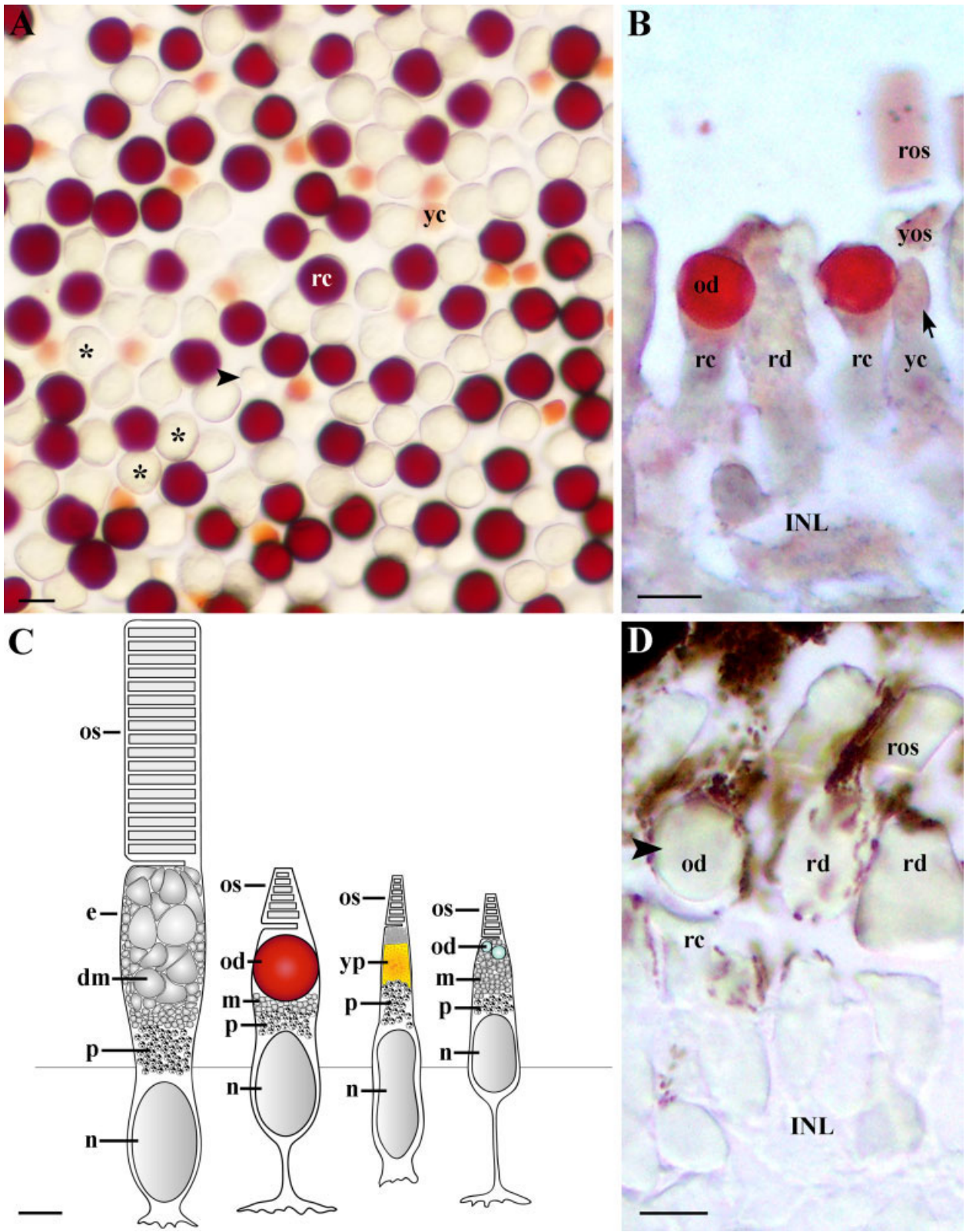

Fig. 2. Morphological characteristics of photoreceptors and lipid histochemistry **A:** Retinal wholemount of a fresh retina showing all four morphological photoreceptor types at the level of the ellipsoid. The large, clear photoreceptors (asterisks) are rods; the red (rc) and yellow (yc) cones are easily distinguishable by the color of their intracellular inclusions. One clear cone (arrowhead) can be identified as it is noticeably smaller than the rod photoreceptors. **B,D:** Oil red O staining of photoreceptor inner segments. Note the strongly positive staining of the oil droplet (od) in red cones (rc) in B. The arrow shows the inner segment of a yellow cone (yc) with no staining. A micrograph of the oil red O control (D) shows that the red droplet color has completely oxidized and faded (arrowhead). **C:** Schematic summary of photoreceptor types in *Neoceratodus forsteri* drawn to scale based on electron and light micrographs of subadults approx. 30–50 cm in TL. Schematic created with Adobe Illustrator 10 (San Jose, CA). dm, distended mitochondria; e, ellipsosome; INL, inner nuclear layer; os, outer segment; p, paraboloid; ros, rod outer segment; yos, outer segment of the yellow cone; yp, yellow pigment. Scale bars = 10 μm in A–D.

TABLE 1. Summary of the Major Intracellular Features of the Four Morphologically Different Photoreceptor Types in *Neoceratodus forsteri*

Morphological feature	Rod	Red cone	Yellow cone	Clear cone
Continuity of the outer segment disks with the extracellular space	−	+	+	+
Oil droplet	−	++ (red)	−	+ (clear)
Nonlipid pigment	−	−	++ (yellow)	−
Distended ellipsoidal mitochondria	++	−	−	+
Paraboloid	++	+	++	+
Location of nucleus in the outer nuclear layer	Vitread	Middle to sclerad	Sclerad	Sclerad
Teleodendrial process	−	++	+	++
Pedicle terminal	−	++	+	++
Spherule terminal	+	−	−	−
Terminal contiguous with the photoreceptor base	+	−	+	−

reveals loosely packed cells containing numerous holes oriented approximately perpendicular to the incident light, where presumably reflective material, i.e., guanine (Nicol et al., 1972) has dissolved away during processing (Fig. 1B). This arrangement constitutes a tapetum lucidum, which we have observed to elicit a pink/red light reflex from the dorsal two-thirds of the fundus in the living eye. A ventral horizontal strip below the tapetum lucidum does not elicit any light reflex and is strongly pigmented. Vitread to the choroid is Bruch's membrane and the retinal pigment epithelial cells (RPEs). The RPE cells extend heavily pigmented processes between all photoreceptors to the level of the external limiting membrane, which is composed of numerous Müller cell end feet.

Morphology and characterization of photoreceptor types

Based on size, morphology, and colored intracellular inclusions, *N. forsteri* possesses at least four morphologically distinct photoreceptor types, a rod and three types (red, yellow, and colorless; referring to the appearance of the intracellular inclusions) of single cone (Figs. 1, 2, Table 1). No double cones are present. Photoreceptors are all assessed in light-adapted retinae, and the incidence of retinomotor movements was not investigated.

Rods. Rods are large (18.62 ± 2.68 μm ellipsoid diameter and 38.22 ± 3.29 outer segment length in a 104-cm TL individual, n = 10) and comprise 53 ± 7% (n = 5) of the total population of photoreceptors. The rod outer segment is cylindrical in shape and in tangential section, and the discs are scalloped, invaginating toward the center to form approx. 20 incisures, all surrounded by the plasma membrane (Fig. 1H). There are many calycal processes running up the entire length of all the photoreceptor types (Fig. 1C). The rod ellipsoid is comprised of packed mitochondria, which become larger (reaching 5 μm diameter in an individual 31.5 cm in TL) and more distended toward the center of the ellipsoid (Fig. 3A,B). The mitochondria are electron-dense with few remaining cristae or any discernible internal structure. Smaller, more electron-lucent mitochondria containing cristae lie laterally and within the vitread end of the ellipsoid. Out of hundreds of electron micrographs examined, one anomalous rod was observed to possess a small oil droplet among the distended mitochondria of the ellipsoid (Fig. 3B). A paraboloid comprised of a dense aggregation of osmiophilic glycogen granules lies immediately beneath the ellipsoidal mitochondria in all rods. The rod nuclei are elongated and often dumb-bell-shaped, more electron-dense than the cone nuclei, and located more vitread in the outer nuclear layer. Two types of rod terminal are present (Fig. 3F,G), the first characterized by an invagination of the base of the perikaryon itself, with no spherule-shaped terminal and up to five synaptic ribbons. The second type is spherule-shaped, protruding from the base of a small teleodendrial process with up to three synaptic ribbons.

Red cones. The most abundant cone type (comprising 35 ± 3% of the total photoreceptor population, n = 6, or 145 ± 97.4 × 10^3 cells in adult retinae, n = 3) contains a large red oil droplet within the ellipsoid of the inner segment, hence the adopted nomenclature of "red cone" (Figs. 1, 2). The outer segment, which is not surrounded by a plasma membrane (Fig. 1G), tapers from a basal diameter of 6.14 ± 0.89 μm (n = 10) in an adult of 104 cm TL. The diameter of the ellipsoid is large (14.26 ± 1.89 μm in a 104-cm TL individual, n = 10) and filled entirely by a red oil droplet, which is bound by a thin membrane that is easily ruptured by tissue processing, i.e., for transmission electron microscopy. In this receptor type, mitochondria lie vitread to the oil droplet, and a small paraboloid of glycogen granules lies above a large (9.6 ± 0.96 μm in diameter, n = 6, in an individual 31.5 cm TL) nucleus, parts of which penetrate the external limiting membrane (ELM; Figs. 1D, 3C). There is no discernible myoid. There is a teleodendrial process at the base of the perikaryon terminating in a synaptic pedicle with up to 10 synaptic ribbons (Fig. 3E).

In some individuals, there is a small crescent-shaped strip (~50 μm wide) of "orange" cones along the temporal edge of some retinae. We believe they represent either a developmental stage of red cones or oxidation of the red cones following enucleation, as they resemble red cones in all other aspects except oil droplet color and have not been seen in any other retinal location except in older, discolored tissue.

Yellow cones. The second most abundant cone type, comprising 9.53 ± 2.52% of the photoreceptor complement (n = 6), contains a granular yellow-orange pigment within the ellipsoid (Figs. 1E, 2A,C). Beneath the cone-shaped outer segment, there is a region of undifferentiated cytoplasm containing rough endoplasmic reticulum, aggregated Golgi apparatus, and small vesicles that resemble diffuse glycogen granules. The most vitread end of the ellipsoidal region is comprised of tightly packed, almost spherical, mitochondria, which appear swollen (Fig. 3D). In fresh (unfixed) tissue, this region is occupied by granular yellow pigment. The myoid contains a large paraboloid of glycogen granules and an elongated nucleus often protruding through the ELM. There are two types of terminal, which project from the base of the yellow cone myoid. The most common type posessess no teleodendrial process, but rather a small pedicle at the end of a spherule-like evagination of the perikaryon, containing up to eight synaptic ribbons (Fig. 3H). The other type is rare

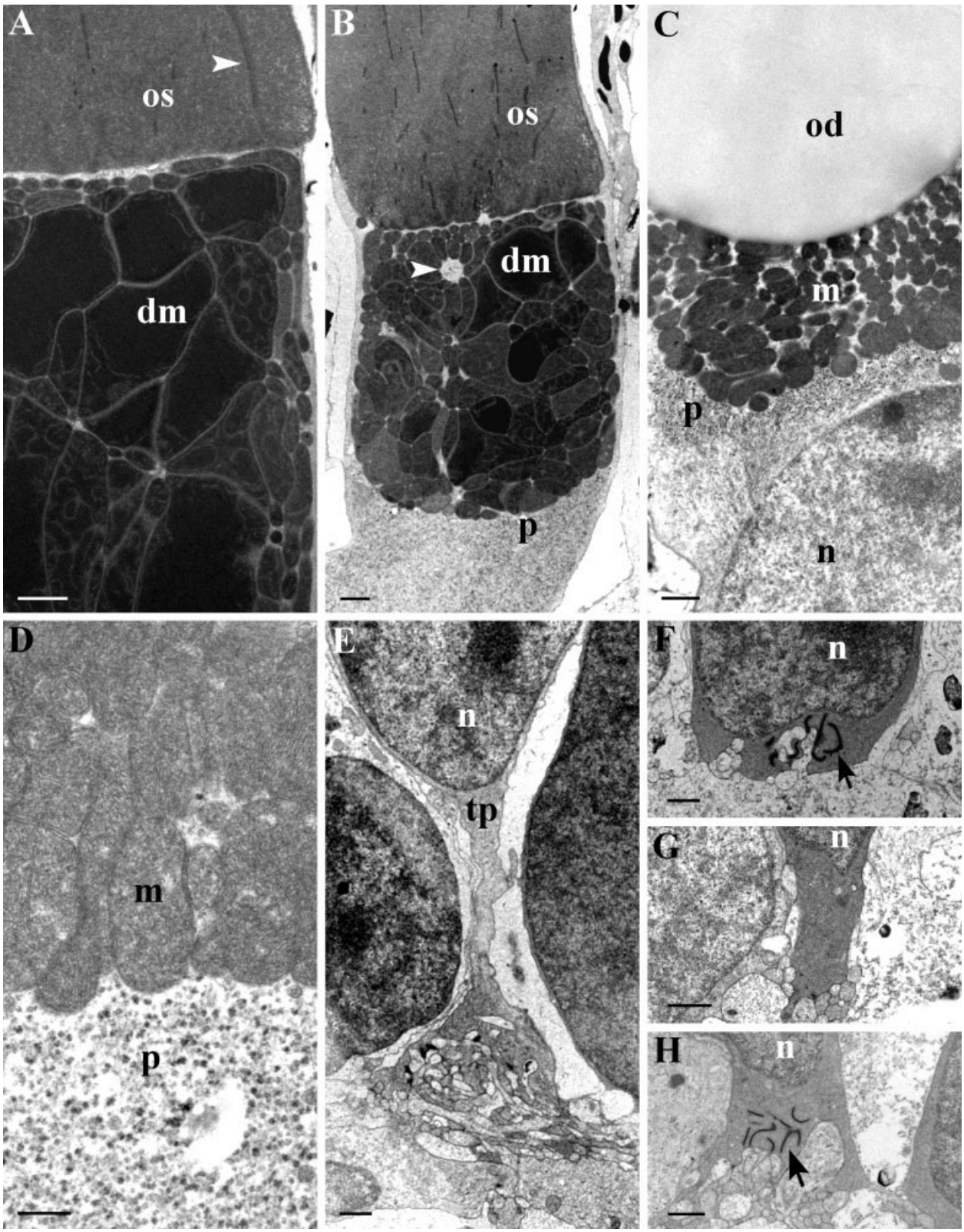

Fig. 3. High-power transmission electron micrographs of juvenile *Neoceratodus forsteri* photoreceptors. **A:** Rod inner segment showing electron-dense, distended mitochondria (dm) with accompanying dissolution of cristae. Arrowhead shows evidence of an incisure in the outer segment (os). **B:** Rod inner segment showing a small oil droplet (arrowhead) embedded within the ellipsoidal mitochondria. **C:** Inner segment of a red cone showing a small paraboloid (p) beneath mitochondria (m) and a large oil droplet (od) filling the ellipsoid. **D:** The inner segment of a yellow cone showing a large paraboloid of glycogen granules. The mitochondria within the yellow cone are more electron lucent than the distended mitochondria seen in rod and clear cone ellipsoids and constitute a yellow pigment in fresh tissue. **E:** A typical red cone terminal forming a pedicle at the end of a teleodendrial process (tp). **F,G:** Two forms of rod terminal; the first type is the most common and comprises an evagination of the base of the perikaryon (F). The second type is more typical of a spherule (G). **H:** A second form of yellow cone terminal is an evagination of the perikaryon similar to the first type of rod terminal but with many more synaptic ribbons visible (arrow). n, nucleus. Scale bars = 1 μm in A–C,E–H; 250 nm in D.

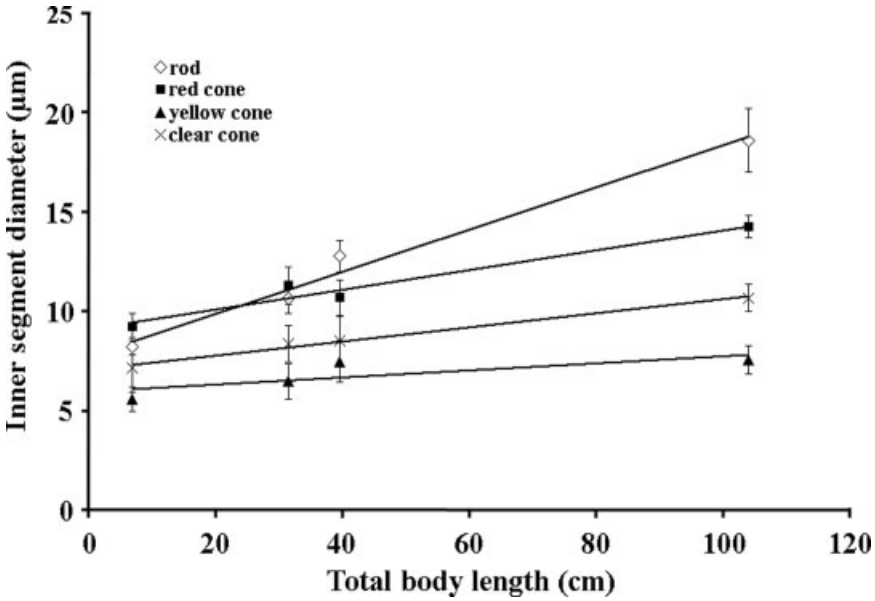

Fig. 4. Photoreceptor inner segment diameter as a function of total length in *Neoceratodus forsteri*. Regression relationships are: rod y = 0.11x + 7.33, $R^2 = 0.97$, $P < 0.014$; red cone y = 0.05x + 8.65, $R^2 = 0.98$, $P < 0.008$; yellow cone y = 0.02x + 5.7, $R^2 = 0.63$, not significant; clear cone y = 0.04x + 6.73, $R^2 = 0.98$, $P < 0.008$.

and comprises a small pedicle containing three synaptic ribbons at the base of a slender (7.4 μm long in an individual 31.5 cm in TL) teleodendrial process.

Colorless cones. The least abundant cone type represents 3.23 ± 0.79% (n = 5) of the total number of photoreceptors, and the ellipsoid diameter is significantly smaller than the ellipsoids of all other photoreceptor types in adults ($P < 0.001$, one-way ANOVA and post hoc Tukey-Kramer test in an individual 104 cm in TL). The ellipsoid contains between one and five small, colorless (in fresh tissue) oil droplets (2.56 ± 1.03 μm in diameter, n = 12, in an individual 31.5 cm in TL) dispersed among mitochondria, which are tightly packed into the inner segment (Figs. 1F, 2A,C). Some of these mitochondria are large and show distension and dissolution of cristae similar to that seen in the rod ellipsoid. The outer segment is small (3.94 ± 0.67 μm long, n = 10, in an individual 31.5 cm in TL), tapering off dramatically from the base of the inner segment. A small paraboloid sits directly above an ovoid nucleus, which is often situated vitread to the external limiting membrane. There is a slender teleodendrial process culminating in a pedicle-shaped terminal.

Lipid histochemistry

In frozen sections, Oil Red O positively stains the large droplet in the most abundant (red) cone type (Fig. 2B,D) and the smaller droplets in the rarest (colorless) cone type. These droplets are therefore composed largely of neutral fats (triglycerides). The ellipsoidal region of the thinner (yellow) cone, corresponding to the localization of yellow pigment in fresh retina, did not positively stain for lipid. Pink staining, indicating the presence of lipids more sparsely distributed than in the oil droplets, was observed in the outer segments of all photoreceptor types and other membranes and axons within the inner retinal layers.

Photoreceptor development

Based on the intracellular features identified in the subadult retina (31.5 cm in TL), all four photoreceptor types are present at all life stages examined in this study (6.8–104 cm TL; Fig. 4). All photoreceptor types, except the yellow cone, increase in diameter in a linear size-dependent relationship (Table 2). The growth of the red oil droplet is closely aligned with the growth of the ellipsoid, as the oil droplet occupies the entire ellipsoidal diameter (abutting the cellular membrane at all growth stages). The colorless oil droplets, however, do not significantly ($P > 0.05$) increase in size during growth. The growth relationship of the rod ellipsoidal diameter is significantly different from that of the cone ellipsoids (ranging from $P < 0.002$ rod to clear cone, to $P < 0.011$ rod to red cone in regression slope comparisons using an unpaired t-test), with the rod diameter more than doubling in size from 8.25 ± 1.43 μm diameter (n = 34 in a 6.8-cm TL individual) to 18.62 ± 2.86 μm diameter (n = 10 in a 104-cm TL individual). During growth, all photoreceptors excluding the colorless cone decreased in density (Table 3). The proportion of each photoreceptor type as a percentage of the total, however, is not significantly different between any retinae at any developmental stage (one-way ANOVA with Tukey-Kramer post hoc test $P > 0.05$ between all combinations).

Spatial resolving power

Based on cone spacing, spatial resolving power increases from 1.57 ± 0.1 cycles degree^{-1} in juveniles (n = 2 individuals 20 cm in TL) to 2.49 cycles degree^{-1} in a subadult (n = 1, 50 cm in TL) and 3.28 ± 0.66 cycles degree^{-1} in adults (n = 3 individuals 98–117 cm in TL). The theoretical spatial resolving power of adult fish is

TABLE 2. Ontogenetic Changes in Photoreceptor Dimensions in *Neoceratodus forsteri*[1]

	Total body length (cm)			
	6.8	31.5	39.5	104
IS diameter (μm)				
Rod	8.25 ± 1.36 (34)	10.65 ± 1.19 (10)	12.79 ± 1.28 (10)	18.62 ± 2.68 (12)
Red cone	9.22 ± 1.43 (20)	11.31 ± 1.49 (10)	10.70 ± 1.50 (11)	14.26 ± 1.89 (43)
Yellow cone	5.61 ± 1.18 (16)	6.48 ± 1.35 (10)	7.49 ± 1.43 (7)	7.59 ± 1.71 (22)
Clear cone	7.14 ± 1.75 (8)	8.38 ± 1.50 (10)	8.54 ± 1.53 (6)	10.69 ± 1.13 (10)
OS length (μm)				
Rod	25.29 ± 6.72 (10)	36.46 ± 2.58 (10)	35.03 ± 3.01 (10)	38.22 ± 3.29 (12)
Red cone	6.93 ± 1.34 (11)	6.80 ± 1.38 (10)	9.95 ± 3.02 (11)	11.54 ± 1.76 (11)
Yellow cone	5.71 ± 1.17 (10)	8.45 ± 2.56 (10)	12.39 ± 2.58 (7)	11.19 ± 2.02 (13)
Clear cone	5.00 ± 2.01 (7)	6.08 ± 1.62 (10)	7.86 ± 2.31 (6)	10.81 ± 1.83 (10)

[1]All values are the mean ± SD, with number of individual cells measured in parentheses. Measurements from electron micrographs in the individuals 6.8 and 31.5 cm in TL have been corrected for shrinkage (5%; see text). Measurements in the individuals 39.5 and 104 cm in TL were made on fresh tissue.

TABLE 3. Density, Total Numbers, and Proportion of Different Photoreceptor Types in Juvenile and Adult *Neoceratodus forsteri*[1]

	Mean cell density (cells × 10^3 mm^{-2})		Peak cell density (cells × 10^3 mm^{-2})		Total cells in retina × 10^3		Proportion representation as % of all photoreceptors		
	Juvenile	Adult	Juvenile	Adult	Juvenile	Adult	Juvenile	Adult	All
All types	6.47 ± 0.59	3.65 ± 0.97	9.28–10.62	3.27–5.21	192 ± 0.95	411 ± 1.80	100	100	100
Rods	3.80 ± 0.20	1.91 ± 0.37	5.25–6.02	2.56–3.94	112 ± 0.54	216 ± 1.94	41.48 ± 1.04	50.88 ± 7.04	47.47 ± 6.56
All cones	2.68 ± 0.18	2.16 ± 0.99	4.55–5.44	2.24–4.99	79 ± 0.63	247 ± 0.98	58.80 ± 2.31	48.53 ± 6.83	53.02 ± 6.88
Red cones	2.16 ± 0.26	1.30 ± 0.53	3.01–4.67	1.60–3.35	64 ± 0.18	145 ± 0.92	33.34 ± 1.03	35.90 ± 4.19	35.13 ± 3.03
Yellow cones	0.43 ± 0.03	0.39 ± 0.16	0.64–0.90	0.63–1.13	12 ± 1.81	43 ± 0.28	6.72 ± 1.10	10.53 ± 1.52	9.53 ± 2.52
Clear cones	0.16 ± 0.02	0.17 ± 0.03	0.32 ± 0.0	0.32–0.79	5 ± 0.0	19 ± 0.33	2.44 ± 0.04	3.28 ± 0.45	3.23 ± 0.79

[1]All values are from wholemounts and are presented as mean ± SD. Data were pooled into juveniles (19 cm in total length, n = 2) and adults (approximately 100 cm in total length, n = 3).

significantly greater than that of juveniles ($P < 0.05$, unpaired t-test), and spatial resolving power increases in a size-dependent linear relationship throughout development (Fig. 5).

Photoreceptor distribution and packing

Photoreceptor density is heterogeneous across the retina, with the distribution of all four morphological photoreceptor types showing regional variation at all stages of development (Figs. 6–8). No geometrically regular photoreceptor mosaic was observed in *N. forsteri* (although a nearest neighbor analysis was not performed; Fig. 2A), but the grouping of specific subpopulations of photoreceptors appears to be nonrandom. Red cones often lie adjacent to each other and are frequently surrounded by five other photoreceptors (of any type). Conversely, yellow and colorless cones rarely lie adjacent to each other but often lie next to a red cone. In our hands, the colors of ellipsoidal inclusions oxidize and fade progressively from the retinal margin toward the center of the retina within 2 days in unfixed or lightly fixed tissue. However, the colors may be maintained for a number of weeks in well-fixed tissue stored in the dark, although, after 2 months, all colors fade from the retina. The process of oxidation appears to be faster in animals that have been bred in captivity.

Rods. In the juvenile and subadult retinae, the area of highest rod cell density (5,504–6,020 cells mm^{-2} in juveniles) lies in the temporal retina (Fig. 6, Table 3). The largest gradient between areae of lowest and highest rod cell density in juveniles is 1:1.96 ± 0.31 (n = 2), with a total of 112 ± 0.54 × 10^3 rods (n =2) in the entire retina. In adults, two areas of increased cell density are located in more central retina, forming a weak horizontal band with a peak of 3,939 cells mm^{-2} (in an adult 100 cm in TL). The gradient from lowest to highest rod cell density in adult retinae is 1:3.20 ± 1.54 (n = 3).

Red cones. The distribution of red cones shows a similar, but subtle, trend at all stages examined. There is a region of increased cell density (with a peak of 1,600–4,670 cells mm^{-2}) in the temporal retina, which lies progressively more ventral as the lungfish matures (Fig. 6). A nasal region of increased cell density is also present at all stages.

Yellow cones. In the juvenile and subadult retinae, a prominent increase (up to 900 cells mm^{-2} in a juvenile 19 cm in TL) in cell density lies within a vertical band in temporal retina, caudal to the optic nerve head (Fig. 7). In adults there is a more pronounced increase in cell density in nasal retina (between 630 and 1,130 cells mm^{-2}).

Colorless cones. In juvenile and adult retinae, there is an increase in cell density in the dorso-temporal retina, with a peak of 320 cells mm^{-2} in juveniles (Fig. 7, Table 3). There is also a gradient increase in the dorso-nasal and nasal retina of varying degrees at all stages. The highest peak of cells in adults lies in ventro-nasal retina (up to 790 cells mm^{-2} in an individual 100 cm in TL).

All cones. The distribution of all cones combined is similar to that of the red cones (Fig. 8). In brief, there is predominantly an increase of cell density in the dorso-temporal retina (with a peak of 4,554–5,440 cells mm^{-2} in juveniles and 2,240–4,992 cells mm^{-2} in adults) and another area of increased cell density in the ventro-nasal retina in all stages.

DISCUSSION

In this investigation we reveal the ultrastructure and heterogeneous distribution of the four morphological photoreceptor types in various developmental stages of *Neoceratodus forsteri*. The retina of *N. forsteri* is adapted for increased scotopic sensitivity while optimizing photopic vision.

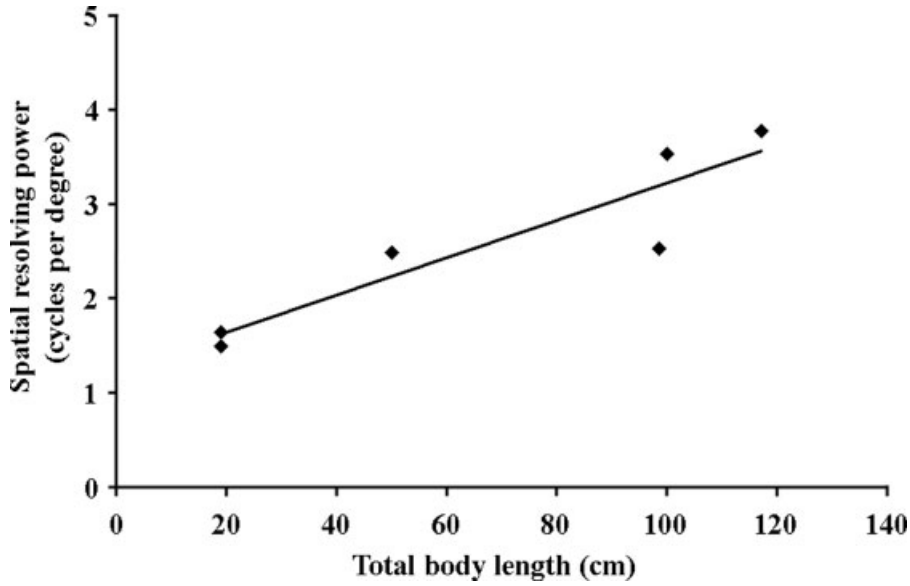

Fig. 5. Ontogenetic change in spatial resolving power from histological measures of cone spacing. Linear regression relationship is $y = 0.02x + 1.24$, $R^2 = 0.85$, $P < 0.009$.

The dipnoan eye

The Australian lungfish *Neoceratodus forsteri* has a small eye in relation to body size (when compared with the logarithmic regression for "typical" fish; Howland et al., 2004; unpublished data) and a thin retina (up to 192.37 ± 11.27 μm thick, n = 5, in a 98-cm adult) compared with most teleosts (Wagner, 1990). The photoreceptors are noticeably large (averaging 18.62 μm and 14.26 μm ellipsoidal diameters in adult rods and cones, respectively). Such large cells would theoretically have a high metabolic requirement, and it is therefore surprising that *N. forsteri* has no retinal or vitreal blood supply or falciform process and must derive all oxygen from the choroidal vasculature (Pow, 1994; this study). This is in contrast to the retina of the African lungfish *Protopterus aethiopicus*, which contains vitreal vessels (Walls, 1942).

N. forsteri possesses a choroidal tapetum lucidum composed of crystal plates (the majority of which are arranged perpendicular to the incident light) across the dorsal two-thirds of the eye. The resultant pink/red colored reflex indicates that the available long-wavelength light penetrating the freshwater environment is reflected back through the photoreceptors to increase sensitivity (Lythgoe, 1972). Interestingly, Nicol et al. (1972) stated that *Lepidosiren paradoxa* does not possess a tapetum, even though they noted that pink light shone through the pupil when the back of the eye was illuminated. Choroidal tapeta are predominantly found in a number of other primitive fishes, e.g., selachians, chimaerids, bichirs, sturgeons, coelacanth, and garfish *Lepisosteus* sp. (Nicol et al., 1972; Wang and Nicol, 1974; Collin and Collin, 1993).

Characterization of photoreceptor types in lungfish

The photoreceptor layer of *N. forsteri* contains at least one type of rod and three types of single cone (red, yellow, and colorless), in accordance with Robinson (1994). Munk (1969) previously identified a rod, a single cone with an oil droplet, and a double cone with an oil droplet within the chief cone, in contrast to this study. An ultrastructural study by Pow (1994) described a rod and a single cone containing a large, clear oil droplet (oxidized examples of red cones in this study). He also described variations of the single cone type containing multiple small oil droplets

Fig. 6. Maps of the distribution of rods and red cones in the retina of *N. forsteri*. Areas shaded lightest gray represent cell density lower than the mean. Intermediate gray represents areas of cell density between the mean, and 1 SD above the mean, whereas areas shaded the darkest gray represent cell density greater than 1 SD above the mean. All calculations are specific to an individual retina. Juvenile (A,E), subadult (B,F), and adult retinae (C,D,G,H). Scale bars = 10 μm. Temporal is to the left, and dorsal is up. A–D: Distribution of rods. In juvenile stages (**A,B**), there is an increased area of cell density in the temporal retina. In adults (**C,D**) the area of increased cell density forms a weak horizontal streak, with the highest peak cell density in nasal retina. Contour boundaries are as follows (cells mm^{-2}):A: <3,500 (lowest 2,560), 3,500–4,410, >4,410 (peak 6,016, asterisk); B: <3,000 (lowest 1,711), 3,000–4,141, >4,141 (peak 5,347, asterisk); C: <2,300 (lowest 897), 2,300–3,011, >3,011 (peak 3,939, asterisk); D: <1,750 (lowest 1,152), 1,750–2,030, >2,030 (peak 2,560, asterisk) **E–H:** The distribution of red cones. There is an area of increased cell density in the temporal retina in all developmental stages, which is where the highest peak cell density is found. There is also an area of increased cell density in the nasal retina. The area of increased cell density extends into the ventral retina as the animal matures **G,H:** Contour boundaries are as follows (cells mm^{-2}):E: <2,000 (lowest 1,472), 2,000–2,342, >2,342 (peak 3,008, asterisk); F: <2,500 (lowest 1,711), 2,500–3,013, >3,013 (peak 3,636, asterisk); G: <2,100 (lowest 1,326), 2,100–2,464, >2,464 (peak 3,354, asterisk); H: <1,456 (lowest 1,020), 1,456–1,672, >1,672 (peak 2,070, asterisk). Scale bars = 10 μm in A–H.

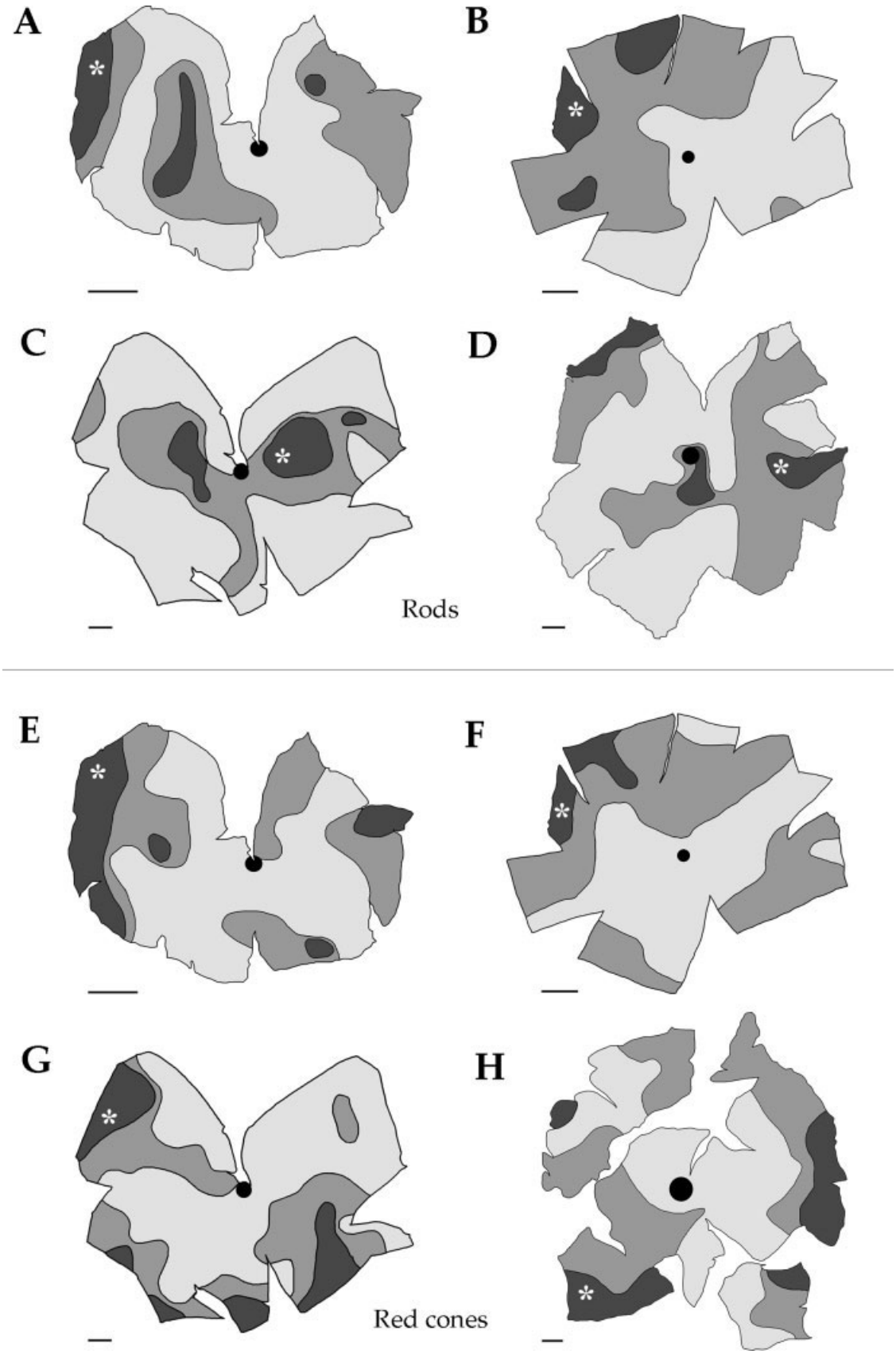

Figure 6

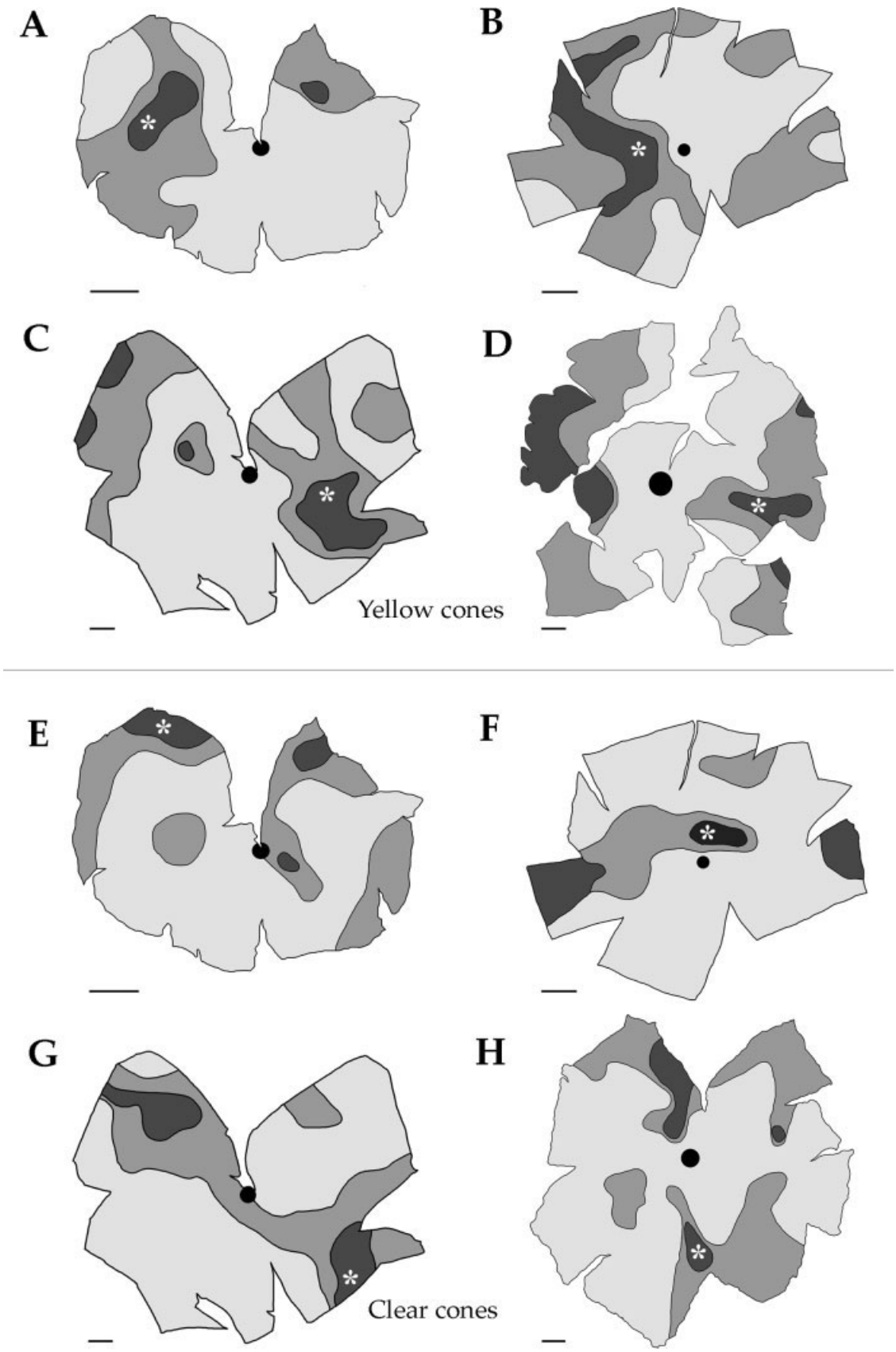

Figure 7

within their inner segment (colorless cones in this study) and cones lacking oil droplets. Pow (1994) speculated that the variations of the single cone with no oil droplet could be components of unequal double cones, or immature cones, which have yet to form oil droplets. Because oil droplets are formed embryologically in the chick *Gallus gallus* and appear in immature cones that are added from the *ora serrata* (Coulombre, 1955; Ishikawa and Yamada, 1969), we conclude that the cone lacking an oil droplet described by Pow (1994) represents the yellow cone described in this study.

Without ultrastructural examination, it is difficult to assess whether the representatives of the other dipnoan species possess the same complement of photoreceptors as *N. forsteri*. Both the African *Protopterus* spp. and the South American *L. paradoxa* possess a rod containing an oil droplet and a paraboloid and a single cone with an oil droplet, whereas *Protopterus* spp. possesses unequal double cones with an oil droplet in the principal member (Walls, 1942; Munk, 1964, 1969; Pfieffer, 1968). Despite previous authors describing unequal double cones in *Protopterus* spp. (Walls, 1942; Munk, 1964, 1969; Pfeiffer, 1968) and *N. forsteri* (Munk, 1964; Pow, 1994), we found no examples of double cones. Munk (1969) described an unequal double cone in *N. forsteri* in which the accessory and principal cones closely resemble the yellow and red cones (Robinson, 1994; this study). This assignation was probably due to the frequent apposition of the yellow and red cones, but ultrastructural investigation confirms the absence of the characteristic subsurface cisternae found along the abutting membranes of double cones in other fishes (Berger, 1967; Le Beux, 1972; Kunz et al., 1983; Wagner, 1990; Collin and Collin, 1998; Shand et al., 1999).

The evolution and function of oil droplets

The intense colors of the red and yellow cones in *N. forsteri* make identification relatively simple. Nicol et al. (1972) described "many small red spheres surrounding groups of yellow refractile circles" while examining the retina of *L. paradoxa*, and red oil droplets have since been recognized in *Protopterus* spp. (Locket, 1999). Colorless oil droplets are present in a number of amphibians (Walls, 1942; Nilsson, 1964) and acipenseriform fishes (Walls, 1942; Munk, 1964, Sillman et al., 1999), and it is believed that the retinal oil droplets in their common ancestor were colored (Walls, 1942). Certain species then lost these colors once a nocturnal existence was adopted and the color was impossible to regain once secondary diurnality occurred (Walls, 1942). This theory was unpopular until the discovery of colored oil droplets in *N. forsteri*, which pushed back the known evolution of colored oil droplets to at least the time of the sarcopterygian emergence in the Devonian, 400 million years ago (Robinson, 1994).

The ellipsoidal droplets of the red and clear cones of *N. forsteri* are oil droplets comprised of lipid, as revealed by their staining with Oil Red O. Conversely, the inner segments of the rods do not contain an oil droplet, unlike the rods of members of the Lepidosirenidae (Kerr, 1902; Rochon-Duvigneaud, 1941; Walls, 1942; Pfeiffer, 1968; Munk, 1969; Ali and Anctil, 1973). Walls (1942) suggested that the presence of an oil droplet and a paraboloid in lepidosirenid rods could indicate they have been more recently derived (via transmutation) from cones. However, genomic DNA and mRNA encoding for the RH1 opsin protein (the rhodopsin characteristic of only rods in other vertebrates) have been isolated in *Protopterus* spp. (Venkatesh et al., 2001) and *N. forsteri* (H.J. Bailes, A.E.O. Trezise, and S.P. Collin, unpublished data), respectively. Therefore, no transmutation from a cone is suspected, but our finding of no positive lipid staining within the rod inner segment of *N. forsteri* may indicate that this oil droplet was lost in the Ceratodontid lineage. Our anomalous finding of a single rod with a small remnant of an oil droplet embedded within the ellipsoidal mitochondria may indicate that it is in the process of being lost from the species and is a derived characteristic of the Dipnoi.

Colored oil droplets in reptiles and birds act as cut-off filters absorbing wavelengths below a certain value (λ cut-off) and thus limit the spectral composition of light available to the visual pigments housed within the outer segment (Liebman and Granda, 1975; Bowmaker and Knowles, 1977; Partridge, 1989). Further work using microspectrophotometry may prove that colored oil droplets in lungfish perform a similar function. Colored oil droplets are composed of neutral lipids and carotenoids (Wald and Zussman, 1937; Meyer et al., 1965; Johnston and Hudson, 1976), whereas the composition of nonlipid pigments, such as that within the yellow cone, is unknown. The nonlipid yellow pigment within the ellipsoid of accessory cones of the eastern box turtle *Emydoidea blandingii* has the same absorbance as yellow oil droplets containing zeaxanthin, and it is assumed the nonlipid yellow pigment is similarly composed of carotenoid (Lipetz, 1984). The fact that oxidation of the color of both the red oil droplet and the yellow pigment in the retina of *N. forsteri* is noticeably

Fig. 7. Maps of the topographic distribution of yellow and clear cones in the retina of *Neoceratodus forsteri*. Areas shaded lightest gray represent cell density lower than the mean. Intermediate gray represents areas of cell density between the mean, and 1 SD above the mean, whereas areas shaded the darkest gray represent cell density greater than 1 SD above the mean. All calculations are specific to an individual retina. Juvenile (A,E), subadult (B,F), and adult retinae (C,D,G,H). Temporal is to the left, and dorsal is up. **A–D:** Distribution of yellow cones: In the juvenile and subadult retinae (A,B), there is an increase in cell density, which forms a vertical band in the temporal retina caudal to the optic nerve head. There is also a less pronounced increase in cell density in nasal retina. Conversely, in later stages (C,D), there is a less pronounced increase in cell density along the temporal edge and a more pronounced increase in cell density in the nasal retina. Contour boundaries are as follows (cells mm^{-2}): A: <450 (lowest 256), 450–612, >612 (peak 896, asterisk); B: <850 (lowest 214), 850–1,204, >1,204 (peak 1,711, asterisk); C: <639 (lowest 234), 639–858, >858 (peak 1,131, asterisk); D: <397 (lowest 153), 397–502, >502 (peak 663, asterisk). **E–H:** Distribution of clear cones. In the juvenile retinae (E), there are increases in cell density in the dorso-temporal and dorso-nasal retina. In the subadult (F), the increased cell density is temporal and nasal, with a prominent small area of higher cell density dorsal to the optic nerve head (asterisk). In adult retinae (G,H), there are also two peripheral areas of increased cell density, but these extend into the ventral and dorsal retina. Contour boundaries are as follows (cells mm^{-2}): E: <150 (lowest 32), 150–220, >220 (peak 320, asterisk); F: <280 (lowest 0), 280–540, 540–795, >795 (peak 1,069, asterisk); G: <170 (lowest 0), 170–325, >325 (peak 788, asterisk); H: <128 (lowest 32), 128–199, >199 (peak 320, asterisk). Scale bars = 10 μm.

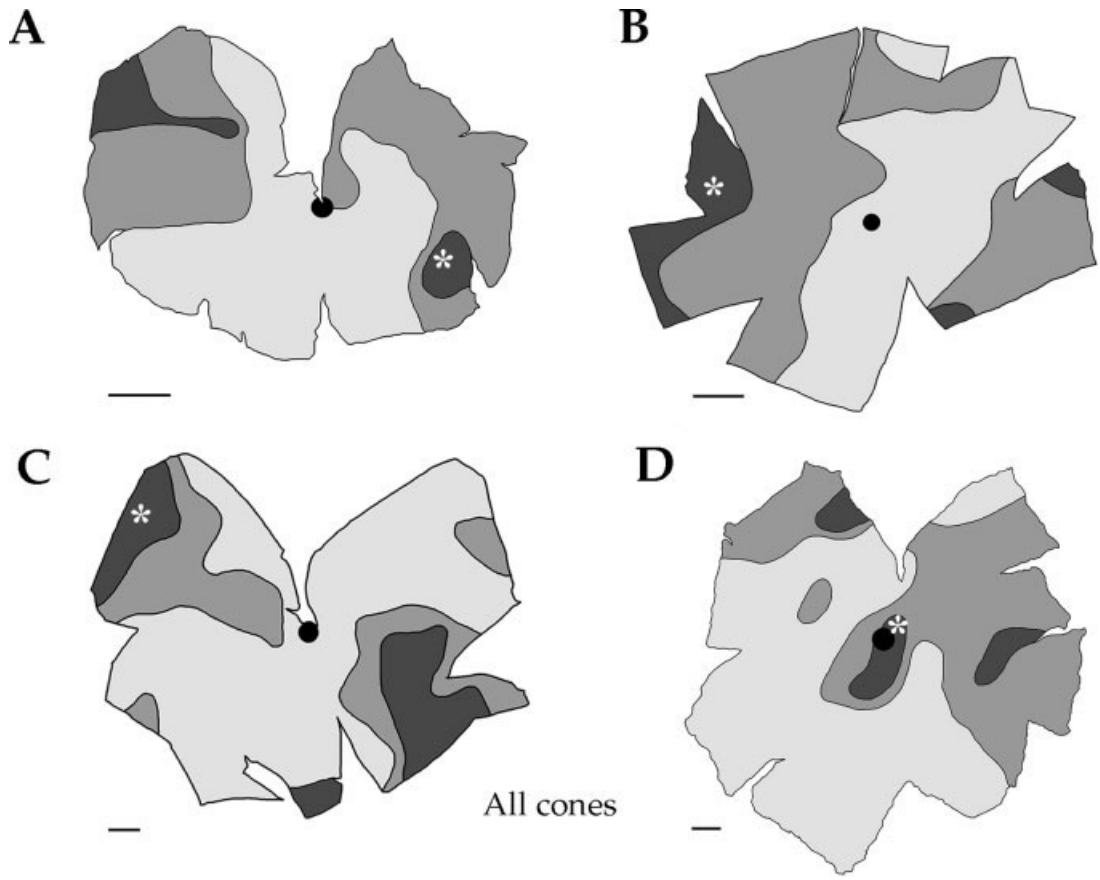

Fig. 8. Maps of the distribution of all cone types in the retina of *Neoceratodus forsteri*. Areas shaded lightest gray represent cell density lower than the mean. Intermediate gray represents areas of cell density between the mean, and 1 SD above the mean, whereas areas shaded the darkest gray represent cell density greater than 1 SD above the mean. All calculations are specific to an individual retina. Juvenile (A,), subadult (B), and adult retinae (C,D). Temporal is to the left, and dorsal is up. Generally, all cones exhibit an increase in cell density in the dorso-temporal and ventro-nasal retina. These two areae would subtend the ventral binocular field in front of the animal, as well as behind and dorsally. Contour boundaries are as follows (cells mm^{-2}): A: <2,500 (lowest 1,728), 2,500–3,061 (peak 4,544, asterisk); B: <3,700 (lowest 2,566), 3,700–4,378, >4,378 (peak 5,562, asterisk); C: <2,900 (lowest 1,989), 2,900–3,448, >3,448 (peak 4,992, asterisk); D: <1,800 (lowest 1,290), 1,800–2,089, >2,089 (peak 2,240, asterisk). Scale bars = 10 μm.

faster in animals bred in captivity suggests that the stability of the colors may be dependent on either the light environment and/or the carotenoid content of their food. Retinal oil droplets of quail (*Coturnix coturnix japonica*) similarly lose all carotenoid pigmentation after being fed a diet lacking carotenoids (Bowmaker et al., 1993).

Colorless oil droplets like those in *N. forsteri* usually form one large droplet and not a number of smaller ones (Kolb and Jones, 1982; Jane and Bowmaker, 1984; Hart et al., 1998; Loew and Govardovskii, 2001). Photoreceptors containing multiple small droplets are unusual. They have previously been described in the pigeon *Columba livia* (Pedler and Boyle, 1969) and some reptiles such as *Phelsuma inunguis* (Pedler and Tansley, 1963), *Elaphe climacaphora* (Ishikawa and Yamada, 1969), and *Thamnophis sirtalis* (Wong, 1989), although these possess multiple (up to hundreds) of small (0.02–0.2 μm in diameter) droplets housed within the one photoreceptor type. The small droplets in *N. forsteri* will be unable to filter all incident light as they do not fill the diameter of the inner segment.

Photoreceptor size and retinal sensitivity

There is a linear relationship between body length and the large rod ellipsoidal diameter in *N. forsteri* (Fig. 6, $y = 0.11x + 7.33$). The largest individual lungfish we have ever caught was 127 cm in TL, and we extrapolate that rods in an animal of this size could reach an average of 21.3 μm in diameter. These rods are, to our knowledge, the widest vertebrate rods ever recorded. The size of the rods of *N. forsteri* eclipses those of other amphibians, e.g., larval *Ambystoma tigrinum* (13 μm in diameter; Mariani, 1986), although their morphology and size shares more similarities with this group than teleost fish. Previous authors have noted similarities between retinal photoreceptor morphology in lepidosirenids and urodele amphibians, highlighting the evolutionary relationship between these groups (Rochon-Duvigneaud, 1941; Pfeiffer, 1968; Locket, 1970a,b; Ali and Anctil, 1973).

The large diameter of the rods of *N. forsteri* suggests high retinal sensitivity, a selective advantage in low light conditions when this species is reportedly more active (Grigg, 1965; Kemp, 1986). Interestingly, the size of the

rods is remarkably similar to the "macroreceptors" (which are 18 μm in diameter) of some species of deep-sea teleosts, e.g., *Scopelarchus* spp., in which sensitivity is increased by grouping large numbers of thin rods (2–3 μm in diameter), which are isolated from their neighbors by guanine tapetal material (Locket, 1971, 1977; Collin et al., 1998). The grouping of rods into macroreceptors, which are thought to be electrically coupled, increases sensitivity by up to 50 times (Locket, 1971).

In addition to large rods, cone ellipsoidal diameters in *N. forsteri* are also large in comparison with other species (14.26 ± 1.89 μm in the red cones in an adult 104 cm in TL, compared with 6.3 ± 0.8 μm in *Polyodon spathula*; Sillman et al., 1999). Van der Meer (1994) suggests that fishes with large cones are able to operate more effectively under low-light conditions as they receive more light-energy per second than smaller cones and has confirmed that a behavioral increase in photopic sensitivity occurs in *Haplochromis sauvagei* as the cones increase in size.

Ontogenetic changes in spatial resolving power

The spatial resolving power of *N. forsteri*, calculated from cone photoreceptor density, is low in comparison witho other fishes but increases ontogenetically from 1.57 ± 0.1 cycles degree^{-1} in juveniles to 3.28 ± 0.66 cycles degree–in adults. In *N. forsteri*, cone photoreceptors are added to the retina throughout development, as has been shown in other fishes and amphibians (Straznicky and Gaze, 1971; Johns and Easter, 1977; Wetts et al., 1989), whereas cone photoreceptor density decreases. Retinal growth is therefore achieved by photoreceptor addition and retinal stretching. An ontogenetic increase in spatial resolving power in *N. forsteri* is achieved by increasing the focal length of the lens with eye growth. Johns and Easter (1977) stated that, in the goldfish *Carassius auratus*, the opposing action of decreasing cell density and lenticular growth should theoretically result in a life-long increase in visual acuity. Behavioral measures of visual acuity in *N. forsteri* are likely to be lower than the histological estimates of spatial resolution calculated here due to the summation of visual signals (Van der Meer, 1995; Collin, 1999), processing by neurons in the inner retina, and the convergence of information onto higher order neurons in the optic tectum (Rahmann, 1979).

Such a low spatial resolving power will have functional constraints on the ability to discriminate detail for *N. forsteri*. Extant Dipnoi are omnivores, and fecal analysis from adult *N. forsteri* has revealed a diet of molluscs, plants, and crustaceans (Kemp et al., 1981). The main mechanism of feeding in lungfish is by suction into the mouth (Bemis, 1986), which is not suggestive of a predatory attack, and we therefore suggest that feeding success involves a combination of sensory systems. It is clear from personal observation that olfaction is important in foraging, and *N. forsteri* can also use electroreception to locate prey in the absence of other cues (Watt et al., 1999).

Topographic specialization and behavior

A temporal increase in rod density in juvenile *N. forsteri* implies an increase in retinal sensitivity for the frontal visual field, useful for the detection of predators (such as invertebrates, fish, and wood duck; Illidge, 1894; Bancroft, 1928). This temporal area of high rod density becomes more central in adults, forming a weak horizontal streak across the retinal meridian and increasing visual sensitivity along the substrate/water interface to aid prey detection at low light levels. Predator avoidance is probably of little importance later on in development.

In addition to a heterogeneous distribution of rods that changes during development and mediates increased scotopic sensitivity, there are also retinal regions of increased cone density in both juvenile and adult *N. forsteri*, which mediate acute photopic vision. The distribution of the total population of cones reveals a peak in dorsotemporal retina (2.24–4.99 × 10^3 receptors mm^{-2} in adults). A similar topographic cone distribution is found in cichlids *Haplochromis elegans* (Van der Meer and Anker, 1984), perch *Perca fluviailitis* (Ahlbert, 1970), killifish *Fundulus heteroclitus* (Flamarique and Harosi, 2000), and goldfish *Carassius auratus* (Mednick et al., 1988) and indicates a downwardly directed visual axis of increased spatial resolving power. Further behavioral investigations may indicate whether there is a functional significance in differential distribution of high-density areas between morphological cone types in *N. forsteri*.

The changes in cone distribution across the retina at various developmental stages are subtle in contrast to changes revealed when teleost fish experience shifts in their visual behavior or visual environment (Kawamura et al., 1984; Evans and Fernald, 1993; Shand, 1997; Beaudet and Hawryshyn, 1999; Shand et al., 1999; Collin et al., 2003). Because the photoreceptors of *N. forsteri* increase in size and number gradually with growth and the overall proportions do not significantly change, the environment inhabited by adults and juveniles is probably similar. This appears to be confirmed, because the few juveniles that have been caught in the Brisbane River were found near weed banks on gravel or sand substrate, a similar environment to that of adults (Grigg, 1965). However, juvenile *N. forsteri* remain elusive in the wild, where recent extensive tagging surveys on the Burnett River using electrofishing techniques have failed to find a significant number of juveniles (Brooks and Kind, 2001). This may be an indication that they frequent other reaches of the river, successfully hiding in among dense macrophytes, or that there is little new recruitment of juveniles into the general population.

CONCLUSIONS

The retina of *N. forsteri* contains at least four morphologically distinct photoreceptor types, whose morphology and size have more in common with extant amphibian retinae than with teleost retinae, perhaps reflecting the unique phylogenetic relationships among the Dipnoi and basal Sarcopterygii. The presence of brightly colored oil droplets suggests a certain degree of diurnal activity, as does the heterogeneous distribution of various cone types across the retina. In addition to mediating increased photopic sensitivity, the retina of *N. forsteri* also possesses specializations for increased scotopic sensitivity, with very large photoreceptors, a tapetum lucidum, and low spatial resolving power.

ACKNOWLEDGMENTS

The authors thank Tina Chua for assistance with processing for scanning electron microscopy. We are grateful

to Paul Manger, Helen Nicoll, Mal Jepson, Kylie Jennings, Nathan Hart, Justin Marshall, and Alan Goldizen for help with collection of animals from the Brisbane and Mary Rivers. We also thank Prof. Jean Joss of Macquarie University and Dr. Ann Kemp of The University of Queensland for their kind donation of captive-bred juvenile animals and Assoc. Prof. Mike Bennett of The University of Queensland for donation of subadults and the use of his large freshwater holding facilities.

LITERATURE CITED

Ahlbert IB. 1970. The organization of the cone cells in the retinae of four teleosts with different feeding habits (*Perca fluviatilis* L., *Lucioperca lucioperca* L., *Acerina cernua* L., & *Coregonus albula* L.). Arkiv F Zool 22:445–481.

Ali MA, Anctil M. 1973. Retina of the South American lungfish *Lepidosiren paradoxa* Fitzinger. Can J Zool 51:969–972.

Bancroft TL. 1928. On the life history of *Ceratodus*. Proc Linn Soc NSW 58:467–469.

Beaudet L, Hawryshyn CW. 1999. Ecological aspects of vertebrate visual ontogeny. In: Archer SN, Djamgoz MBA, Loew ER, Partridge JC, Vallerga S, eitors. Adaptive mechanisms in the ecology of vision. Dordrecht: Kluwer Academic Publishers. p 413–437.

Beaudet L, Novales Flamarique I, Hawawryshyn C. 1997. Cone photoreceptor topography in the retina of sexually mature pacific salmonid fishes. J Comp Neurol 383:49–59.

Bemis WE. 1986. Feeding systems of living Dipnoi: anatomy and function. J Morphol Suppl 1:249–275.

Berger ER. 1967. Subsurface membranes in paired cone photoreceptor inner segments of adult and neonate *Lebistes* retinae. J Ultrastruct Res 17:226–232.

Bowmaker JK, Knowles A. 1977. The visual pigments and oil droplets of the chicken retina. Vision Res 17:755–764.

Bowmaker JK, Kovach JK, Whitmore AV, Loew ER. 1993. Visual pigments and oil droplets in genetically manipulated and carotenoid deprived quail—a microspectrophotometric study. Vision Res 33:571–578.

Brinkmann H, Venkatesh B, Brenner S, Meyer A. 2004. Nuclear protein-coding genes support lungfish and not the coelacanth as the closest living relatives of land vertebrates. Proc Natl Acad Sci U S A 101:4899–4905.

Broin Fd, Buffetaut E, Koenigueur J-C, Russell D, Taquet P, Vergnaud-Grazzini C, Wenz S. 1974. La faune de vert&eacutebrés continentaux du gisement d'In Beceten (Sénonien du Niger). C R Biol 279:469–472.

Brooks S, Kind P. 2001. Ecology and demographics of lungfish (*Neoceratodus forsteri*) and general fish communities in the Burnett River, Queensland, with reference to the impacts of Walla Weir and future infrastrcture development. Brisbane, Australia: Queensland Department of Primary Industries Report, Queensland Government.

Collin SP. 1999. Behavioural ecology and retinal cell topography. In: Archer SN, Djamgoz MBA, Loew ER, Partridge JC, Vallerga S, editors. Adaptive mechanisms in the ecology of vision. Dordrecht: Kluwer Academic Publishers. p 509–535.

Collin SP, Collin HB. 1993. The visual system of the Florida garfish *Lepisosteus platyrhinchus* (Ginglymodi) I. Retina. Brain Behav Evol 42:77–97.

Collin SP, Collin HB. 1998. Retinal and lenticular ultrastructure in the aestivating salamanderfish, *Lepidogalaxias salamandroides* (Galaxiidae, Teleostei) with special reference to a new type of photoreceptor mosaic. Histol Histopathol 13:1037–1048.

Collin SP, Hoskins RV, Partridge JC. 1998. Seven retinal specializations in the tubular eye of the deep-sea pearleye, *Scopelarchus michaelsarsi*: a case study in visual optimization. Brain Behav Evol 51:291–314.

Collin SP, Hart NS, Shand J, Potter IC. 2003. Morphology and spectral absorption characteristics of retinal photoreceptors in the southern hemisphere lamprey (*Geotria australis*). Vis Neurosci 20:119–130.

Coulombre AJ. 1955. Correlations of structural and biochemical changes in the developing retina of the chick. Am J Anat 9:153–189.

Dean B. 1906. Notes on the living specimens of the Australian lungfish, *Ceratodus forsteri*, in the Zoological Society's collection. Proc Zool Soc Lond 1906:168–178.

Evans BI, Fernald RD. 1993. Retinal transformation at metamorphosis in the winter flounder (*Pseudopleuronectes americanus*). Vis Neurosci 10:1055–1064.

Flamarique IN, Harosi FI. 2000. Photoreceptors, visual pigments, and ellipsosomes in the killifish, *Fundulus heteroclitus*: a microspectrophotometric and histological study. Vis Neurosci 17:403–420.

Grigg GC. 1965. Studies on the Queensland lungfish, *Neoceratodus forsteri* (Krefft). III. Aerial respiration in relation to habits. Aust J Zool 13: 413–421.

Hart NS, Partridge JC, Cuthill IC. 1998. Visual pigments, oil droplets and cone photoreceptor distribution in the European starling (*Sturnus vulgaris*). J Exp Biol 201:1433–1446.

Howland HC, Merola S, Basarab JR. 2004. The allometry and scaling of the size of vertebrate eyes. Vision Res 44:2043–2065.

Illidge T. 1894. On *Ceratodus forsteri*. Proc R Soc Qld 10:40–44.

Ishikawa T, Yamada E. 1969. Atypical mitochondria in the ellipsoid of the photoreceptor cells of vertebrate retinas. Invest Ophthalmol 8:302–316.

Jane SD, Bowmaker JK. 1984. A microspectrophotometric study of the visual pigments and oil droplets found in the retina of the Aylesbury duck (*Anas platyrynchos domesticus*). Vision Res 24:1701–1702.

Johns PR, Easter SSJ. 1977. Growth of the adult goldfish eye. II. Increase in retinal cell numbers. J Comp Neurol 176:331–342.

Johnston D, Hudson RA. 1976. Isolation and composition of carotenoid-containing oil droplets from cone photoreceptors. Biochim Biophys Acta 424:235–245.

Joss JMP, Cramp N, Baverstock PR, Johnson AM. 1991. A phylogenetic comparison of 18s-ribosomal RNA sequences of lungfish with those of other chordates. Aust J Zool 39:509–518.

Kawamura G, Tsuda R, Kumai H, Ohasi S. 1984. The visual cell morphology of *Pagrus major* and its adaptive changes with shift from pelagic to benthic habitats. Bull Jpn Soc Sci Fish 50:1975–1980.

Kemp A. 1986. The biology of the Australian lungfish, *Neoceratodus forsteri* (Krefft 1870). J Morphol Suppl 1:181–198.

Kemp A, Molnar RE. 1981. *Neoceratodus forsteri* from the lower Cretaceous of New South Wales, Australia. J. Palaeontol. 55:211–217.

Kemp A, Anderson T, Tomley A, Johnson I. 1981. The use of the Australian lungfish (*Neoceratodus forsteri*) for the control of submerged aquatic weeds. In: C.S.I.R.O., editor. 5th International Conference on Weed Control. Melbourne: C.S.I.R.O. p 155–158.

Kerr JG. 1902. The development of *Lepidosiren paradoxa*. III. Development of the skin and its derivatives. Q J Microsc Sci 46:417–406.

Kolb H, Jones J. 1982. Light and electron microscopy of the photoreceptors in the retina of the red-eared slider *Pseudemys scripta elegans*. J Comp Neurol 209:331–338.

Kunz YW, Ennis S, Wise C. 1983. Ontogeny of the photoreceptors in the embryonic retina of the viviparous guppy, *Poecilia reticulata*, P. (Teleostei). Cell Tissue Res 230:469–486.

Le Beux YJ. 1972. Subsurface cisterns and lamellar bodies: particular forms of endoplasmic reticulum in the neurons. Z Zellforsch Mikrosk Anat 133:327–352.

Liebman PA, Granda AM. 1975. Super dense carotenoid spectra resolved in single cone oil droplets. Nature 253:370–372.

Lillie RD, Ashburn LL. 1943. Super-saturated solutions of fat stains in dilute isopropanol for demonstration of acute fatty degenerations not shown by the Herxheimer technique. Arch. Pathol 36:432–440.

Lipetz LE. 1984. Pigment types, densities and concentrations in cone oil droplets of *Emydoidea blandingii*. Vision Res 24:597–604.

Locket NA. 1970a. Landolt's club in the retina of the African lungfish, *Protopterus aethiopicus* Heckel. Vision Res 10:299–306.

Locket NA. 1970b. Mitosis in mature lungfish retina. Zool J Linn Soc 49:1–4.

Locket NA. 1971. Retinal anatomy in some scopelarchid deep-sea fishes. Proc R Soc Lond B Biol Sci 178:161–184.

Locket NA. 1977. Adaptations to the deep-sea environment. In: Crescitelli F, editor. Handbook of sensory physiology. Berlin: Springer. p 67–192.

Locket NA. 1999. Vertebrate photoreceptors. In: Archer SN, Djamgoz MBA, Loew ER, Partridge JC, Vallerga S, editors. Adaptive mechanisms in the ecology of vision. Dordrecht: Kluwer Academic Publishers. p 163–196.

Loew ER, Govardovskii VI. 2001. Photoreceptors and visual pigments in the red-eared turtle, *Trachemys scripta elegans*. Vis Neurosci 18:753–757.

Lythgoe JN. 1972. The adaptation of visual pigments to the photic envi-

ronment. In: Dartnall HJA, editor. Handbook of sensory physiology: photochemistry of vision. Berlin: Springer-Verlag. p 567–603.

Mariani AP. 1986. Photoreceptors of the larval tiger salamander retina. Proc R Soc Lond B Biol Sci 227:483–492.

Marshall CR. 1986. A list of fossil and extant Dipnoans. J Morphol Suppl 1:15–23.

Matthiessen L. 1880. Untersuchungen über dem aplanatismus und die periscopie der kristallinsen in den augen der fische. Pflugers Arch 21:287–307.

Mednick AS, Berk MF, Springer AD. 1988. Asymmetric distribution of cells in the inner nuclear and cone mosaic layers of the goldfish retina. Neurosci Lett 94:241–246.

Meyer DB, Cooper TG, Gernez C. 1965. The structure of the eye: retinal oil droplets. In: Rohen JW, editor. The structure of the eye. Stuttgart: Schattauer. p 521–533.

Moy-Thomas JA, Miles RS. 1971. Palaeozoic fishes. Philadelphia: WB Saunders. p 140–160.

Munk O. 1964. The eye of *Calamoichthyes calabaricus* Smith, 1865 (Polypteridae, Pisces) compared with the eye of other fishes. Vidensk Medd Dansk Naturh Foren Bd 127:113–125.

Munk O. 1969. On the visual cells of some primitive fishes with particular regard to the classification of rods and cones. Vidensk Medd Dansk Naturh Foren Bd 132:25–30.

Nicol JAC, Arnott HJ, Best ACG. 1972. Tapeta lucida in bony fishes (Actinopterygii): a survey. Can J Zool 51:69–81.

Nilsson SEG. 1964. An electron microscopic classification of the retinal receptors of the leopard frog (*Rana pipiens*). J Ultrastruct Res 10:390–416.

Partridge JC. 1989. The visual ecology of avian cone oil droplets. J Comp Physiol A 165:415–426.

Pedler C, Boyle M. 1969. Multiple oil droplets in the photoreceptors of the pigeon. Vision Res 9:525–528.

Pedler C, Tansley K. 1963. The fine structure of the cone of a diurnal gecko (*Phelsuma inunguis*). Exp Eye Res 2:39–47.

Pfeiffer W. 1968. Retina und Retinomotorik der Dipnoi und Brachiopterygii. Z Zellforsch 89:62–72.

Pow DV. 1994. Taurine, amino-acid transmitters, and related molecules in the retina of the Australian lungfish *Neoceratodus forsteri*—a light-microscopic immunocytochemical and electron-microscopic study. Cell Tissue Res 278:311–326.

Rahmann HG. 1979. Ontogeny of visual acuity of rainbow trout under normal conditions and light deprivation. Brain Behav Evol 68:315–322.

Rasband WS. 1997–2005. Image J. Bethesda, MD: US National Institutes of Health.

Robinson SR. 1994. Early vertebrate color-vision. Nature 367:121–121.

Rochon-Duvigneaud A. 1941. L'oeil de *Lepidoseran paradoxa*. CR Biol 212:307–309.

Schiefferdecker P. 1886. Studien zur vergleichenden Histologie der Retina. Arch Mikrosk Anat 28:305–396.

Shand J. 1997. Ontogenetic changes in retinal structure and visual acuity: a comparative study of coral-reef teleosts with differeing post-settlement lifestyles. Environ Biol Fish 49:307–322.

Shand J, Archer MA, Collin SP. 1999. Ontogenetic changes in the retinal photoreceptor mosaic in a fish, the black bream, *Acanthopagrus butcheri*. J Comp Neurol 412:203–217.

Sige B. 1968. Dents de micromammifidres et fragments de coquilles d'oeufs de Dinosauriens dans la faune de Vertébrés du Crétace supérieur de Laguna Umayo (Andes péruviennes). CR Acad Sci Paris D 267:1495–1498.

Sillman AJ, O'Leary CJ, Tarantino CD, Loew ER. 1999. The photoreceptors and visual pigments of two species of Acipenseriformes, the shovelnose sturgeon (*Scaphirhynchus platorynchus*) and the paddlefish (*Polyodon spathula*). J Comp Physiol A Sens Neural Behav Physiol 184:37–47.

Simpson R, Kind P, Brooks S. 2002. Trials of the Queensland lungfish. Nat Aust 2002:36–43.

Stone J. 1981. The wholemount handbook. Sydney: Maitland.

Straznicky K, Gaze RM. 1971. The growth of the retina in *Xenopus laevis*: an autoradiographic study. J Embryol Exp Morphol 26:67–79.

Takezaki N, Figueroa F, Zaleska-Rutczynska Z, Takahata N. 2004. The phylogenetic relationship of tetrapod, coelacanth, and lungfish revealed by the sequences of 44 nuclear genes. Mol Biol Evol 21:1512–1524.

Tamura T. 1957. A study of visual perception in fish, especially on resolving power and accommodation. Bull Jpn Soc Sci Fish 22:536–557.

Tohyama Y, Ichimiya T, Kasama-Yoshida H, Cao Y, Hasegawa M, Kojima H, Tamai Y, Kurihara T. 2000. Phylogenetic relation of lungfish indicated by the amino acid sequence of myelin DM20. Mol Brain Res 80:256–259.

Van der Meer HJ. 1994. Ontogenic change of visual thresholds in the cichlid fish *Haplochromis sauvagei*. Brain Behav Evol 44:40–49.

Van der Meer HJ. 1995. Visual resolution during growth in a cichlid fish: a morphological and behavioural case study. Brain Behav Evol 45:25–33.

Van der Meer HJ, Anker GC. 1984. Retinal resolving power and sensitivity of the photopic system in seven haplochromine species (Teleostei, Cichlidae). Neth J Zool 31:197–209.

Venkatesh B, Mark EV, Brenner S. 2001. Molecular synapomorphies resolve evolutionary relationships of extant jawed vertebrates. Proc Natl Acad Sci U S A 98:11382–11387.

Wagner H-J. 1990. Retinal structure of fishes. In: Douglas RH, Djamgoz MBA, editors. The visual system of fish. London: Chapman and Hall. p 109–157.

Wald G, Zussman H. 1937. Carotenoids of the chicken retina. Nature 140:197.

Walls G. 1942. The vertebrate eye and its adaptive radiation. New York: Hafner Publishing Company.

Wang RT, Nicol JAC. 1974. The tapetum lucidum of gars (Lepisosteidae) and its role as a reflector. Can J Zool 52:1523–1530.

Watt M, Evans CS, Joss JMP. 1999. Use of electroreception during foraging by the Australian lungfish. Anim Behav 58:1039–1045.

Wetts R, Serbezija GN, Fraser SE. 1989. Cell lineage analysis reveals multipotent precursors in the ciliary margin of the frog retina. Dev Biol 136:254–263.

Wong ROL. 1989. Morphology and distribution of neurons in the retina of the American garter snake *Thamnophis sirtalis*. J Comp Neurol 283: 587–601.

Yokobori S, Hasegawa M, Ueda T, Okada N, Nishikawa K, Watanabe K. 1994. Relationship among coelacanths, lungfishes, and tetrapods—a phylogenetic analysis based on mitochondrial cytochrome-oxidase I gene sequences. J Mol Evol 38:602–609.

Zardoya R, Cao Y, Hasegawa M, Meyer A. 1998. Searching for the closest living relative(s) of tetrapods through evolutionary anlayses of mitochondrial and nuclear data. Mol Biol Evol 15:506–517.